Journal of Alloys and Compounds 707 (2017) 51–56

Contents lists available at ScienceDirect

Journal of Alloys and Compounds

journal homepage: http://www.elsevier.com/locate/jalcom

Influence of Tb on structure and properties of Fe-19%Ga and Fe-27%Ga alloys

I.S. Golovin [a, *], A.M. Balagurov [b], V.V. Palacheva [a], A. Emdadi [a], I.A. Bobrikov [b], A.Yu Churyumov [a], V.V. Cheverikin [a], A.V. Pozdniakov [a], A.V. Mikhaylovskaya [a], S.A. Golovin [c]

[a] National University of Science and Technology "MISIS", Leninsky Ave. 4, 119049 Moscow, Russia
[b] Frank Laboratory of Neutron Physics, Joint Institute for Nuclear Research, 141980 Dubna, Russia
[c] Tula State University, Lenin Ave. 84, 300012 Tula, Russia

ARTICLE INFO

Article history:
Received 24 July 2016
Received in revised form
26 August 2016
Accepted 15 September 2016
Available online 16 September 2016

Keywords:
Fe-Ga alloy
Phase transitions
Magnetic and anelastic properties
Neutron diffraction

ABSTRACT

Influence of microalloying by Tb on structure and some properties of Fe-19%Ga and Fe-27%Ga type alloys is studied. 0.1%Tb increases magnetostriction of water quenched Fe-19%Ga alloy with A2 structure from 120 to 210 ppm (1.75-fold). Slow cooling decreases magnetostriction in both Tb-free and Tb-doped alloys. Microalloying by Tb increases magnetostriction and influences on phase transitions in the Fe-27Ga type alloys in the range of 20–750 °C as observed by *in situ* neutron diffraction and vibrating sample magnetometry. The conventional transition sequence of phase transitions at heating $D0_3 \rightarrow L1_2 \rightarrow D0_{19} \rightarrow B2 \rightarrow A2$ in binary Fe-27Ga is changed for $D0_3 \rightarrow B2 \rightarrow B2 + L1_2 \rightarrow B2 + D0_{19} \rightarrow B2 \rightarrow A2$ transitions in the Tb-containing alloy. The increase in Tb content from 0.15% to 0.3% decreases the amount of closed packed phases. At slow cooling (2 K/min), the mixture of $D0_3 + L1_2$ is recorded in the Tb-containing sample instead of dominating $L1_2$(~90%) and a very limited amount of $D0_{19}$ and A2 phases in the binary Fe-27Ga alloy. This influence of Tb on the phase transition kinetics explains temperature dependent magnetization curves with step by step accumulation of the $L1_2$ phase in subsequent heating and cooling cycles. Thus, we conclude that the additions of Tb stabilize bcc-born phases (A2, B2 and $D0_3$) and prevents the appearance of closed packed (fcc ordered $L1_2$ and hcp ordered $D0_{19}$) phases, which contributes to the functional properties of that alloys.

1. Introduction

Rare-earth elements (such as Tb, Dy, etc.) exhibit a huge Joule magnetostriction [1] due to their substantial spin-orbit interaction, though only at low temperatures. That is why, alloys between rare-earths and 3d-elements are often considered for magnetostrictive applications [2]. Recently rare-earth-free Fe-Ga alloys have also become a focus of research because of their highest magnetostriction among Fe-based alloys [3]. In addition to a good saturated magnetostrictive response (λ_S ~ 400 ppm in single crystal form) under very low magnetic fields (~8 kA/m), Fe-Ga alloys possess good mechanical properties making them a sustainable alternative especially to conventional Terfenol-D that suffers from brittleness and low yield stress under shock and tensile loads. Desirable mechanical properties and relatively low switching field have introduced Fe-Ga alloys as a promising class of smart magnetostrictive materials for sonar systems, acoustic sensors and transducers, actuators, positioning devices, torque sensors, and recently developed magnetoelectric (or multiferroic) sensors and transducers [4,5]. Fe-Ga alloys exhibit a relatively high damping capacity at low [6] and high [7] frequencies of vibrations due to irreversible motion of magnetic domain walls and eddy currents, correspondingly.

Doping with a third element alters the magnetostriction of Fe-Ga alloys. Doping with interstitial elements B, C, and N marginally increases the magnetostriction [8–10] whereas alloying with the 3d and 4d transition elements, such as Ni, V, Cr, Mn, Co, Mo, and Rh reduces the magnetostriction [11–14]. Based on the idea that strong localized magnetocrystalline anisotropy is associated with a giant magnetostriction, rare earth elements were recently proposed to

* Corresponding author.
E-mail address: i.golovin@misis.ru (I.S. Golovin).

http://dx.doi.org/10.1016/j.jallcom.2016.09.151
0925-8388/

dope the FeGa alloys [15–18]. An increase in the magnetostriction from 70 to 160 ppm and from 35 to 90 ppm was recorded respectively in polycrystalline $Fe_{83}Ga_{17}Tb_{0.2}$ [17] and $Fe_{81}Ga_{19}Tb_{0.3}$ [18] alloys. The giant perpendicular magnetostriction up to −886 ppm and −800 ppm was achieved in Tb- and Ce-doped melt-spun ribbons [15,19].

Fe-Ga binary alloys have two maxima of magnetostriction at 17–19 and ~27 at.% Ga (atomic percentage is used in this paper) [20]. Mechanical and magnetic properties of the Fe-(17–19)Ga alloys have been studied much better compared to Fe-27Ga alloys in which several phase transitions take place. Up till now no results have been reported about the effect of Tb on functional properties of Fe-27Ga alloys except for our own paper [21]. Therefore, the main purpose of this paper is to study the effect of Tb on the type and kinetics of phase transitions in Fe-27Ga alloys. We use *in situ* neutron diffraction to study sequence and kinetics of phase transitions in directly solidified Fe-27.4Ga, Fe-27.4Ga-0.3 Tb, and Fe-26.2Ga-0.15 Tb alloys. The paper focuses on the differences in the phase transformations in bulk samples with and without Tb upon heating and cooling.

2. Materials and methods

Fe-19 at.%Ga and Fe-27 at.%Ga type alloys with 0.10–0.30 at.%Tb were produced by directional solidification in copper mould using pure Fe and Ga by induction melting under protection of high-purity inert argon gas using an Indutherm MC–20 V mini furnace. Using energy dispersive spectroscopy, the chemical compositions of the cast buttons were measured with ±0.2% accuracy.

Phase transitions in these alloys were *in situ* characterized by neutron diffraction patterns measured with a high resolution Fourier diffractometer (HRFD) [22] at the IBR-2 pulsed reactor in JINR (Dubna). The tests were performed on rectangular samples with a size of 4 × 8 × 40 mm. The acquisition time for each diffraction pattern was as short as 1 min. Heating of the samples was carried out in a specialized furnace (ILL standard) with vanadium screens up to 850 °C with a temperature rate of ~2.2 K/min. Further details can be found in Refs. [23,24].

The microstructure of the alloys was studied by means of a scanning electron microscopy (SEM) operating at 20 kV using a TESCAN VEGA LMH microscope with a LaB6 cathode and an energy dispersive X-ray microanalysis system (Oxford Instruments Advanced AZtecEnergy). Both backscattered electron and secondary electron imaging were used in the analysis. The statistical error of the detector for the determination of element concentrations using X-ray analysis is 0.2 wt%. The EBSD analysis of the alloys was investigated using the NordlysMax2 detector (Oxford Instruments Advanced AZtecEnergy). The MAD was 0.5.

Magnetic properties (magnetization, magnetostriction) were recorded using a vibrating sample magnetometer VSM-130 up to 750 °C with a heating rate of 6 K/min and field ~800 kA/m, and a hand-made experimental setup based on a strain gauge method up to saturated magnetic field value of 35 kA/m. The thermal analysis (DSC) was done using a Labsys Setaram system with heating rates from 10 to 30 K/min.

3. Results

3.1. Fe-19Ga based alloys

Fig. 1a shows magnetostriction for Fe-19%Ga and 0.1%Tb-doped Fe-19%Ga as a function of a magnetic field at different heat treatment states. For the Fe-19%Ga alloy, the saturation magnetostriction (λ_S) approaches 120 and 80 ppm, respectively, for the water quenched and furnace cooled samples. These values are considerably lower than those measured in our previous work for the alloy with nearly the same composition [25]. The ingot used in our earlier paper was produced using a directional solidification technique, and the samples for magnetostriction tests were cut along relatively long columnar grains. In contrast, the current samples were cut in the perpendicular direction to the growth direction. Thus, having more grain boundaries along the direction of magnetostriction tests, the samples exhibited lower magnetostriction. This finding explains the difference between λ_S values measured in those two papers. At this stage, we are focused on the contribution of Tb into phase transitions and the change in magnetic properties than absolute values of magnetostriction. We also assume that noticeable discrepancy between magnetostrictions reported by several researchers [e. g. [15, 17, 18]] for similar Fe-Ga compositions after similar heat treatment is also related to the differences in the production method and the direction in which the samples are cut for measurement. According to Fig. 1a, doping with 0.1 at.% of Tb not only increases the saturation magnetostrictive (λ_S) but also affects the slope of the magnetostriction versus the applied magnetic field. Tb significantly enhances the λ_S of Fe-19Ga alloy: from 120 to 210 ppm in a water quenched state and from 85 to 195 ppm in a furnace cooled state. An increase in the slope of the λ(H) curves corresponds to an increase in magnetic permeability, which is particularly desirable for practical sensor or actuator applications [26]. In both parent and Tb-doped 19%Ga galfenol, water quenching leads to higher λ_S values, whereas furnace cooling noticeably decreases λ_S by 15 ppm (7%) and 35 ppm (30%) for parent and doped Fe-19Ga alloy. Water quenching suppresses the formation of ordered phases and enhances magnetostriction in Fe-Ga alloys, whereas furnace cooling triggers precipitation of $D0_3$ and $L1_2$ ordered structures. Magnetostriction for Fe-27Ga type alloys is presented in (Fig. 1b), and is discussed below.

The water quenched Fe-19Ga alloy has rather quite a regular magnetic domain (MD) structure as compared with the as-cast Fe-27Ga alloy, though both samples have a rather similar phase structure (A2 or $D0_3$). It was reported that introducing a higher amount of Ga decreases the degree of regularity of MD structures [27]. Water quenching can also contribute towards an increase in the degree of alignment of MD structures in the Fe-19Ga alloy. Doping with Tb modifies the MD structures of the Fe-27Ga alloy. Adding Tb increases magneto-crystalline anisotropy energy in the Fe-Ga alloys [16,19,28]. These results are also consistent with the magnetostriction results (Fig. 1b) showing that Tb-doped Fe-27Ga with aligned MD structures has significantly higher magnetostriction than Tb-free Fe-27Ga with irregular MD structures. Furnace cooling leads to the formation of irregular maze-like MD structures in Fe-19Ga (Fig. 1d), which may be, at least partly, the result of the precipitation of the ordered phase.

Fig. 2a shows XRD reflection patterns for Tb-free and Tb-containing Fe-19Ga alloy. A dominating bcc A2 structure of the α-iron is identified for both samples in as-cast state with the characteristic peaks indexed to (110), (200), (211), (220), and (310) reflection planes. Asymmetric peaks observed at higher degrees result from $D0_3$ ordering of A2 phase as reported in Ref. [25]. No reflections from Tb-rich precipitates were detected in contrast with [15,17], in which the formation of Ga_6Tb phase in Fe-17Ga-0.4Tb alloy was reported. Slightly [110]-preferred crystallographic orientation of parent alloys retains in Tb doped alloy. Our results show an increase in relative intensity of the (200) reflection for Fe-19.5Ga-0.1Tb sample, which is consistent with the papers [15,17] that report that a significant amount of Tb favors the distribution along the [200] axis in Tb-doped Fe-Ga alloys.

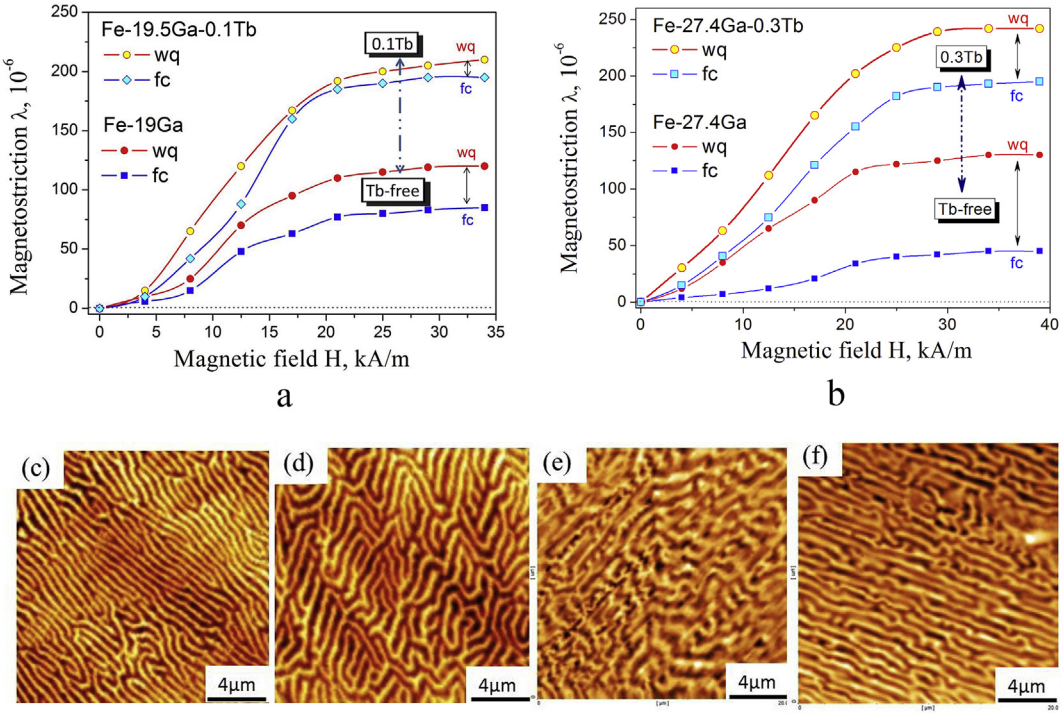

Fig. 1. (a) Magnetostriction as a function of a magnetic field for water quenched and furnace cooled Fe-19Ga (a) and Fe-27Ga (b) samples. Typical magnetic domain images of water quenched (c) and furnace cooled (d) Fe-19Ga alloy, and of as-cast Fe-27.6Ga (e) and as-cast Fe-27.4Ga-0.3Tb (f) alloys.

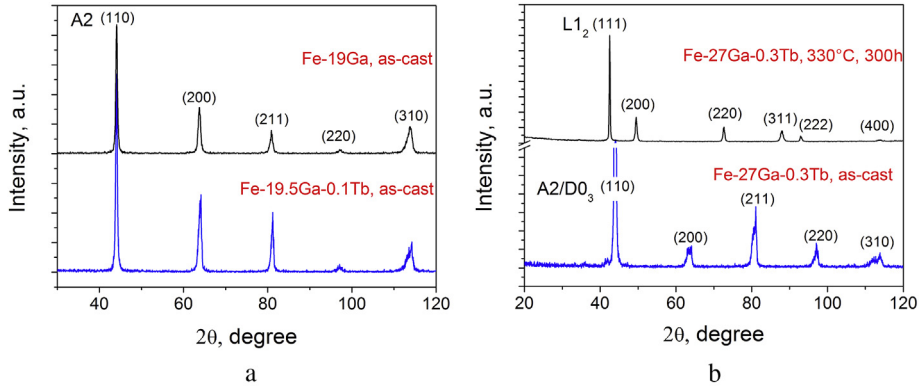

Fig. 2. (a) Room temperature X-ray diffraction spectra of parent and doped Fe-19Ga in the cast state and (b) Fe-27Ga-0.3 Tb in the as cast state and after 300 h annealing at 330 °C.

3.2. Fe-27Ga-Tb alloys

Addition of Tb in the Fe-27Ga alloys increases the magnetostriction of the alloys (Fig. 1b). The saturation magnetostriction is higher after water quenching as compared with the furnace cooled samples. Absolute values of the saturation magnetostriction for the Fe-27Ga alloys are higher than those for the Fe-19Ga alloys.

Temperature dependence of the magnetization of the as cast Fe-27Ga alloy is presented in Fig. 3a (the blue curve). A decrease of the magnetization up to about ~450 °C relates to a decrease of ferromagnetism of the $D0_3$ phase. However, a direct observation of this dependence up to zero magnetization (i.e., to the Curie temperature) is hardly possible, as the $D0_3$ phase itself transforms to the $L1_2$ phase in this temperature range: see below the neutron diffraction data (Figs. 4 and 5). An increase in the magnetization above ~450 °C is due to the formation of a ferromagnetic $L1_2$ phase (the $L1_2$ phase has a Cu_3Au-type structure with Fe and Ga atoms partially ordered, sp. gr. $Pm3m$, $a \approx 3.72$ Å at 20 °C). Finally, the magnetization decreases above 620 °C due to the $L1_2 \rightarrow D0_{19}$ transition ($MgCd_3$-type structure with Fe and Ga atoms partially ordered, sp. gr. $P6_3/mmc$, $a \approx 5.28$ Å, $c \approx 4.28$ Å at 20 °C). At cooling, a monotonous growth of the magnetization takes place practically to the initial level instead of some accumulation of the $L1_2$ phase after each heating and cooling cycle.

Temperature dependence of the magnetization of the as cast ternary Fe-26Ga-0.15Tb alloy (Fig. 3a, red curve) is qualitatively similar to the binary alloy, but the qualitatively magnetization due to the $L1_2$ phase is about four times lower than that of in the binary alloy: <40 emu/g instead of ~130 emu/g in the binary alloy. The magnetization at 500–600 °C, i.e., in the range of the $L1_2$ phase existence, increases in several subsequent heating–cooling cycles, proving an increase in the $L1_2$ phase volume fraction in each cycle of heating-and-cooling. A certain deviation from a smooth behaviour of the magnetization at about 200 °C both at heating and

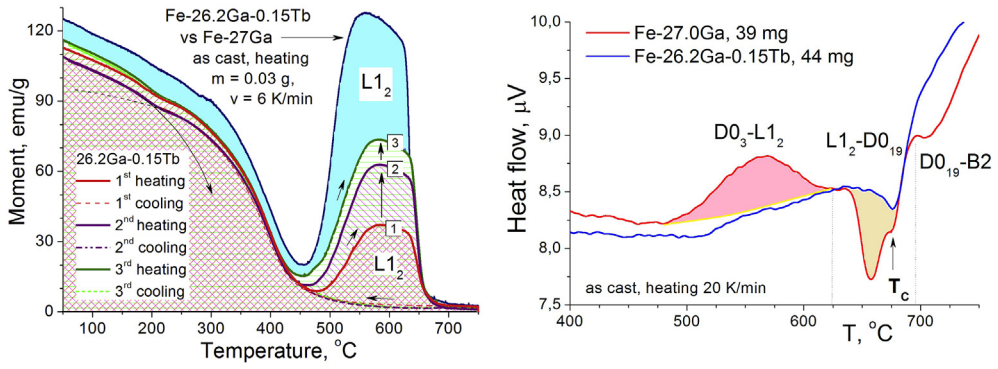

Fig. 3. Temperature dependent magnetization with a heating/cooling rate of 6 K/min (a) and a heat flow with a heating rate of 20 K/min (b) for the Fe-27Ga and Fe-26.2Ga-0.15 Tb as cast alloys. The magnetization curves for the Fe-26.2Ga-0.15 Tb alloy are shown for three subsequent heating-and-cooling cycles.

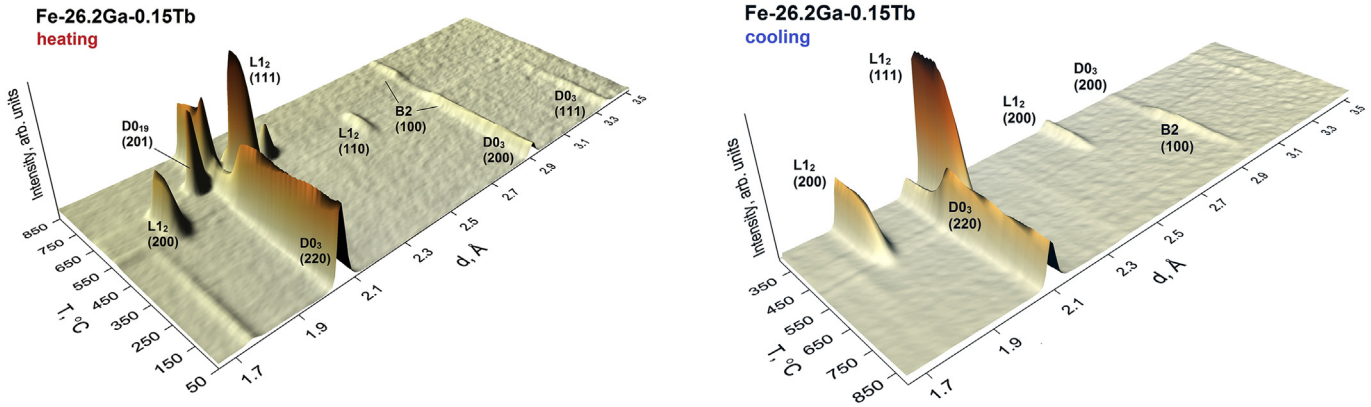

Fig. 4. The 3D visualization of the diffraction pattern upon heating (a) and subsequent cooling (b) the Fe-26.2Ga-0.15 Tb sample after direct solidification.

cooling is not yet completely clear: This effect at first heating of the as cast or water quenched sample might be explained by A2 → $D0_3$ ordering and annihilation of as quenched vacancies recorded in our previous papers ([29] and [30], correspondingly), but hardly in the next subsequent heating and cooling cycles.

Heat flow tests also demonstrate effects for the $D0_3$ → $L1_2$ → $D0_{19}$ → B2 transitions in the binary alloys whereas in the ternary Fe-26Ga-0.15 Tb alloy, they are practically not detectable at a heating rate of 20 K/min (Fig. 3b).

According to neutron diffractions, the initial state after direct solidification for the Fe-27Ga [23] and the Fe-26Ga-0.15 Tb (this paper) samples is represented by the bcc-born $D0_3$ structure (ordered A2 phase), which has a BiF_3-type structure with Fe and Ga atoms partially ordered, sp. gr. $Fm3m$, $a \approx 5.83$ Å at 20 °C. The widths of the diffraction lines only slightly exceed the contribution from the resolution function, which agrees with our earlier findings [23,24]. This conclusion is different from the papers [29,30], though it does not contradict it: we found a mixture of the A2 and $D0_3$ phases in the Fe-26.3Ga and Fe-27.4Ga alloys by XRD. In contrast with the XRD diffractions from most rapidly cooled surfaces of the sample, the neutron diffraction is recorded from the bulk samples which cooling rate is lower. Thus, we can conclude that only a very thin surface area of the samples has a disordered A2 structure, whereas in the bulk sample, $D0_3$ ordering takes place.

Upon heating and cooling, several phase transitions occur. Fig. 4 shows their 3D representation for the ternary Fe-26.2Ga-0.15Tb sample. The d-spacing range from 1.65 to 3.50 Å is shown. The initial state is the $D0_3$ phase identified by (200) and (111) lines at $d = 2.92$ Å and 3.37 Å. Vanishing of the (111) line at heating and its subsequent appearance at cooling (both at about 500°C) means $D0_3$ ↔ B2 transformation.

This 3D overview of the phase transitions is quite different as compared to the representation of the phase transitions in the binary Fe-27Ga alloy [23]. The main difference between the phase transitions in the binary and ternary alloys is in the amount of intermediate phases appeared between the initial ($D0_3$) at room temperature and the final (A2) state at 850 °C at heating and also in the final state after cooling. The recorded sequence of the phase transitions upon continuous heating in the Fe-27Ga alloy is: $D0_3$ → $L1_2$ → $D0_{19}$ → B2 → A2 [23]; whereas in the Fe-27Ga-Tb alloys, this sequence is $D0_3$ → $L1_2$ + A2 → $D0_{19}$ + A2 → B2 → A2 (Fig. 5). The amount of the closed packed phases ($L1_2$ and $D0_{19}$) significantly decreases with an increase in Tb content from 0.15 to 0.3 at.%.

In the Fe-27Ga sample, continuous cooling (after heating up to 850 °C to 100% A2 structure) leads to the formation of the $L1_2$ phase directly from the A2 phase below 550 °C. Some limited amount of the $D0_{19}$ appears in the temperature range from 560 to 460 °C practically simultaneous with the $L1_2$ phase, and a certain amount of the A2 phase remains down to room temperature. This sequence is different for the ternary alloys: for the alloy containing 0.15%Tb the appearance of the $L1_2$ phase takes place, but no $D0_{19}$ phase is detected and a bigger amount of the A2 phase remains up to room temperature. For the ternary alloy with 0.3%Tb [21], only very limited amount of the $L1_2$ phase appears at cooling, whereas the bcc-born $D0_3$ phase remains to be the dominating phase in the structure after furnace cooling: the high temperature A2 phase gets

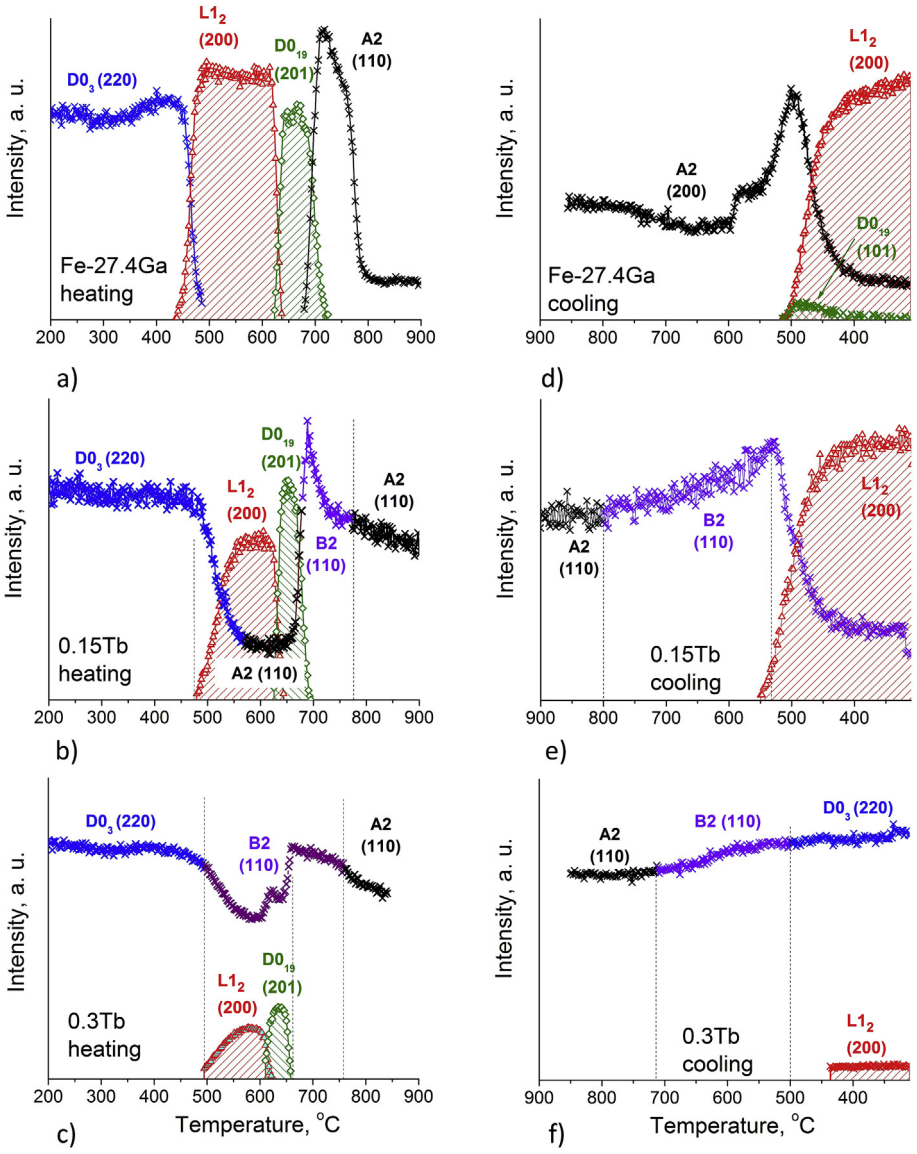

Fig. 5. Phase transitions in the Fe-27Ga (a, d) and Fe-27Ga-Tb with 0.15 (b, e) and 0.3 (c, f) at.% at heating (a, b, c) and cooling (d, e, f) with a rate of ~2.2 K/min shown as intensity changes of the characteristic diffraction peaks. The Miller indices of the peaks are indicated nearby the curves.

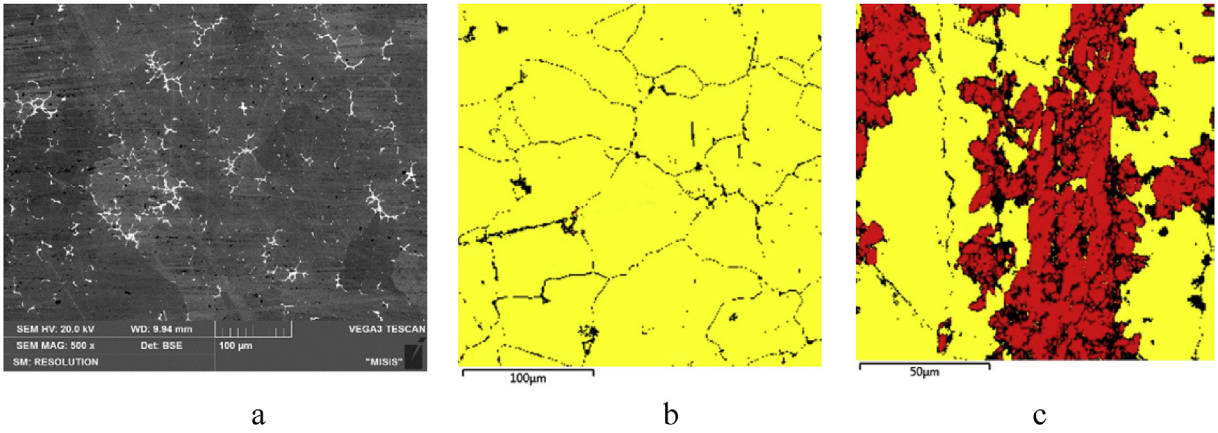

Fig. 6. The microstructure (a) and the EBSD analysis (b) of the Fe-27Ga-0.3 Tb alloy in the cast state and after annealing at 330 °C, 300 h (c) (yellow colour - D0$_3$ phase, red colour - L1$_2$ phase, black colour – Tb-rich phase). (For interpretation of the references to colour in this figure legend, the reader is referred to the web version of this article.)

first B2 ordering between 700 and 500 °C and then $D0_3$ ordering below 500 °C.

Obviously, the volume fraction of the phases at heating and cooling if estimated by intensities of neutron reflections, significantly depends on the texture in the alloys. Nevertheless, our comparative study of bulk and powdered Fe-Ga samples of the same composition showed that this factor is not strong enough to influence our conclusions [31].

At least some reasons for the Tb influence on slowing down kinetics of the phase transitions in the Fe-27Ga alloys can be found with the help of scanning electron microscopy. The SEM study shows a certain competition between precipitation of the Tb-enriched phase (average Tb content in this phase is about 6–9 at.%, rough estimation of volume fraction is 5–7%) and nucleation of the $L1_2$ phase: both prefers grain boundaries in the as cast alloys. Nevertheless, the Tb-enriched phase already precipitates in the as cast state (Fig. 6a,b). At subsequent annealing, these precipitations prevent nucleation of the $L1_2$ phase. Long-term annealing of the as cast sample at 330 °C shows that the $L1_2/D0_3$ boundaries that appeared during annealing are practically free from the Tb-rich phase, whereas the Tb-rich phase decorates original grain boundaries in the as cast sample (Fig. 6c).

4. Conclusions

An improvement of the functional properties of the Fe-Ga alloy by adding a small amount of terbium reported in several papers is confirmed in this paper for alloys with 19 and 27%Ga. An increase in Tb content in Fe-27Ga type alloys from 0.15 to 0.3 at.% progressively suppresses those phase transitions which lead to the appearance of closed packed phases ($L1_2$ and $D0_{19}$) at heating, cooling, and isothermal annealing. Tb also influence ordering of the A2 phase during furnace cooling: in the Tb-free, sample we obtained a bcc A2 structure, whereas in the sample with 0.15%Tb, the B2 ordering of the bcc phase takes place and in the sample with 0.3%Tb further ordering to the $D0_3$ structure takes place.

The Tb-rich phase (up to 9 at.%Tb) precipitates on the grain boundaries of the as cast sample and suppresses nucleation of the $L1_2$ phase on the grain boundaries. In contrast, grain boundaries between the $D0_3$ and $L1_2$ phase that appears at further annealing are free from Tb-rich precipitates.

Acknowledgements

I.S.G. gratefully acknowledges the financial support of Increase Competitiveness Program of MISiS and DAAD grant No.: 91573930 (2015), V.V.P. - DAAD grant No.: 57214227 (2016), and Dr. E. Bazanova for her critical reading of the manuscript. This study is supported by Ministry of Science and Education, Russia, State task to Universities #1855.

References

[1] J.P. Joule, Philos. Mag. 30 (1847) 76–87.
[2] R. Grössinger, R. Sato Turtelli, N. Mehmood, IOP Conf. Ser. Mater. Sci. Eng. 60 (2014) 012002.
[3] A.E. Clark, K.B. Hathaway, M. Wun-Fogle, J.B. Restorff, T.A. Lograsso, V.M. Keppens, G. Petculescu, R.A. Taylor, J. Appl. Phys. 93 (2003) 8621–8623.
[4] J. Atulasimha, A.B. Flatau, Smart Mater. Struct. 20 (2011) 043001.
[5] N. Srisukhumbowornchai, S. Guruswamy, J. Appl. Phys. 90 (2001) 5680.
[6] I.S. Golovin, V.V. Palacheva, V.Yu Zadorozhnyy, J. Zhu, H. Jiang, J. Cirfe, T.A. Lograsso, Acta Mater. 78 (2014) 93–102.
[7] S.U. Jen, Y.Y. Lo, L.W. Pai, J. Phys. D. Appl. Phys. 49 (2016) 145004.
[8] M. Huang, T.A. Lograsso, A.E. Clark, J.B. Restorff, M. Wun-Fogle, J. Appl. Phys. 103 (2008) 07B314.
[9] S.M. Na, A.B. Flatau, J. Appl. Phys. 103 (2008) 07D304.
[10] A.E. Clark, J.B. Restorff, M. Wun-Fogle, K.B. Hathaway, T.A. Lograsso, M. Huang, E. Summers, J. Appl. Phys. 101 (2007) 09C507.
[11] A.E. Clark, M. Wun-Fogle, J.B. Restorff, T.A. Lograsso, G. Petculescu, J. Appl. Phys. 95 (2004) 6942–6943.
[12] P. Mungsantisuk, R.P. Corson, S. Guruswamy, J. Appl. Phys. 98 (2005) 123907.
[13] C. Bormio-Nunes, R. Sato Turtelli, H. Mueller, R. Grössinger, H. Sassik, M.A. Tirelli, J. Magn. Magn. Mater. 290 (2005) 820–822.
[14] E.M. Summers, T.A. Lograsso, M. Wun-Fogle, J. Mater. Sci. 42 (2007) 9582–9594.
[15] W. Wu, J. Liu, C. Jiang, J. Alloys Compd. 622 (2015) 379–383.
[16] W. Wu, J. Liu, C. Jiang, H. Xu, 103 (2013) 262403.
[17] L. Jiang, J. Yang, H. Hao, G. Zhang, S. Wu, et al., Appl. Phys. Lett. 102 (2013) 222409.
[18] T.I. Fitchorov, S. Benneta, L. Jiang, G. Zhang, Z. Zhao, Y. Chen, V.G. Harris, Acta Mater. 73 (2014) 19–26.
[19] Y. He, C. Jiang, W. Wu, B. Wang, H. Duan, H. Wang, T. Zhang, J. Wang, J. Liu, Z. Zhang, P. Stamenov, J.M.D. Coey, H. Xu, Acta Mater. 109 (2016) 177–186.
[20] Q. Xing, Y. Du, R.J. McQueeney, T.A. Lograsso, Acta Mater 56 (2008) 4536–4546.
[21] A.M. Balagurov, I.A. Bobrikov, I.S. Golovin, V.V. Cheverikin, S.A. Golovin, Mater. Lett. 181 (2016) 67–70.
[22] A.M. Balagurov, Neutron News 16 (2005) 8–11.
[23] I.S. Golovin, A.M. Balagurov, V.V. Palacheva, I.A. Bobrikov, V.B. Zlokazov, Mater. Des. 98 (2016) 113–119.
[24] I.S. Golovin, A.M. Balagurov, I.A. Bobrikov, J. Cifre, J. Alloys Compd. 688 (2016) 310–319.
[25] A.A. Emdadi, J. Cifre, O.Yu Dementeva, I.S. Golovin, J. Alloys Compd. 619 (2015) 58–65.
[26] Y. Chen, S.M. Gillette, T. Fitchorov, L. Jiang, H. Hao, J. Li, X. Gao, A. Geiler, C. Vittoria, V.G. Harris, Appl. Phys. Lett. 99 (2011) 042505.
[27] F. Bai, J. Li, D. Viehland, J. Appl. Phys. 98 (2005) 023904.
[28] T. Ma, S. Hu, G. Bai, M. Yan, Y. Lu, H. Li, X. Peng, X. Ren, Appl. Phys. Lett. 106 (2015) 112401.
[29] I.S. Golovin, V.V. Palacheva, A.I. Bazlov, J. Cifre, N. Nollmann, S.V. Divinski, G. Wilde, J. Alloys Compd. 656 (2016) 897–902.
[30] L. Dubov, Yu Shtotsky, Yu Akmalova, Yu Funticov, V. Palacheva, A. Bazlov, I.S. Golovin, Mater. Lett. 171 (2016) 46–49.
[31] A.M. Balagurov, I.S. Golovin, I.A. Bobrikov, V.V. Palacheva, V.B. Zlokazov, Submitted.